Journal of
Mechanics of
Materials and Structures

ON SMALL AZIMUTHAL SHEAR DEFORMATION OF FIBRE-REINFORCED CYLINDRICAL TUBES

Mohamed A. Dagher and Kostas P. Soldatos

Volume 6, No. 1-4 January–June 2011

mathematical sciences publishers

JOURNAL OF MECHANICS OF MATERIALS AND STRUCTURES
Vol. 6, No. 1-4, 2011

ON SMALL AZIMUTHAL SHEAR DEFORMATION OF FIBRE-REINFORCED CYLINDRICAL TUBES

MOHAMED A. DAGHER AND KOSTAS P. SOLDATOS

The problem of azimuthal shear deformation of a transversely isotropic elastic circular cylindrical tube is considered and studied in the small deformation regime. The preferred direction of the transverse isotropy is assumed to lie on the plane of the tube cross-section and is due to the existence of a single family of plane spiral fibres. Consideration of the manner that either the tube material or the fibres may be constrained gives rise to four different versions of the problem which are all susceptible to an exact closed form solution when fibres are perfectly flexible. Particular attention is paid to the special case of straight fibres aligned along the radial direction of the tube cross-section, where comparisons are made between the aforementioned solution obtained when fibres are perfectly flexible and a corresponding solution obtained when fibres posses bending stiffness. It is found that the conventional linear elasticity considerations associated with the perfectly flexible fibre assumption cannot adequately account for the effects of material anisotropy. In contrast, effects of material anisotropy can be accounted for when fibres posses bending stiffness, by taking into consideration the action of couple-stress and therefore asymmetric stress. Moreover, an intrinsic material length parameter which appears naturally in the associated governing equations may be chosen as a representative of the fibre thickness in this case. It is also seen that deformation patterns of fibres possessing bending stiffness as well as corresponding stress distributions developed within the tube cross-section fit physical expectation much closer than their perfectly flexible fibre counterparts.

1. Introduction

The classical version of the problem of azimuthal shear deformation of an elastic circular cylindrical tube of infinite extent is due to Rivlin [1949] and, in several forms and variations, has been considered and studied afterwards by several investigators. This refers to a particular, plane-strain type of finite strain which is applied on the cross-section of an incompressible isotropic hyper-elastic circular cylindrical tube of infinite extent. Accordingly, under the action of an appropriate set of boundary conditions, the tube cross-section is subjected to pure azimuthal shear strain during which it remains circular while its inner and outer radii do not change. A comprehensive review of the relevant literature was presented recently in [Kassianidis et al. 2008], which introduced further and dealt with a new version of this problem; namely the case in which the incompressible material of the tube exhibits some kind of anisotropy. In some detail, the tube cross-section was considered to be reinforced by a single family of unidirectional extensible fibres; this consideration furnished the tube material with properties of transverse isotropy.

Dagher's work was supported through a PhD scholarship awarded by the Egyptian Ministry of Higher Education.
Keywords: anisotropic elasticity, azimuthal shear strain, fibre bending stiffness, fibre-reinforced materials, linear elasticity, transverse isotropy.

Most recently, a second family of plane extensible fibres was placed on the tube cross-section [Dorfmann et al. 2010], thus assuming that the anisotropy of the material of interest proceeds beyond the relatively simple symmetries of transverse isotropy. As already implied, the directions of preference considered in either this latter paper or [Kassianidis et al. 2008] were assumed capable to extend or contract considerably, allowing thus the incompressible material of the tube to withstand the imposed conditions of pure azimuthal shear deformation.

A relevant problem was also considered recently in [Soldatos 2010], as an application of a study having as principal purpose to investigate the influence that some new, second gradient effects have on finite plane deformations of ideal fibre-reinforced hyper-elastic solids. That problem dealt with azimuthal shear strain of an incompressible hyper-elastic circular cylindrical tube having its cross-section reinforced by a single family of inextensible fibres (see also [Soldatos 2009a]); recall that an incompressible material which is further reinforced by one or more families of inextensible fibres is known as ideal fibre-reinforced material (see [Spencer 1972], for example). The new development in [Soldatos 2009a; 2010] made clear that pure azimuthal shear strain is not possible when the incompressible material of the tube contains an inextensible direction of transverse isotropy. Unlike [Kassianidis et al. 2008] where extension or contraction of fibres is assumed possible, a single family of inextensible fibres causes change of both the inner and outer tube radii in a manner that preserves the area of the tube cross-section. It is noted in passing that, since the cross-sectional area remains also unchanged under conditions of pure azimuthal shear strain, the latter kind of deformation [Rivlin 1949; Kassianidis et al. 2008; Dorfmann et al. 2010] becomes essentially a particular case of the outlined "area-preserving" azimuthal shear strain of a circular cylindrical tube.

The new, second gradient deformation effects that [Soldatos 2010] is mainly interested on are relevant with the ability of fibres to resist bending. However, the described "area-preserving" azimuthal shear deformation was found attainable by the ideal fibre-reinforced material considered in [Soldatos 2010] regardless of whether the inextensible fibres involved possess bending stiffness or not (in the latter case fibres are assumed perfectly flexible). The analysis in [Soldatos 2009a; 2010] revealed further that, if the inextensible fibres involved are initially straight and aligned along the radial direction of the tube cross-section, they remain straight during deformation and force the tube to undergo area-preserving azimuthal shear strain by changing their slope only. Some link was therefore observed between the strength of fibres in extension or contraction and their ability to resist bending. It was accordingly concluded that, if the direction of transverse isotropy is due to the existence of strong fibres, the tube should be expected to resist the conditions of pure azimuthal shear deformation. Instead, tendency will be observed for creation of a deformation pattern that couples azimuthal shear strain and radial stretching. Moreover, fibre bending stiffness should be dominant in the formation of such a pattern.

It is instructive at this point to mention that the principal problem met in nature is essentially the problem in which the transversely isotropic material of the tube is completely unconstrained. Hence, by employing the concept of the ideal fibre-reinforced material, the references [Soldatos 2009a; 2010] dealt essentially with a first approximation to the solution of the finite azimuthal shear strain problem of a fibre-reinforced cylindrical tube. Many materials are of course nearly incompressible and, similarly, many kinds of natural or structural fibres are nearly inextensible. Hence, in many cases of interest, either the incompressible material considered in [Kassianidis et al. 2008] or a compressible material reinforced by inextensible fibres yields a realistic and plausible simplification of the principal problem. Either case

is regarded as an intermediate step between the latter problem and that considered in [Soldatos 2009a; 2010] for a corresponding doubly constrained material. Further progress in the subject should therefore consider to dismiss one or both of the material constraints involved in these two references.

Dismissal of the fibre inextensibility constraint leads to the comprehensive relevant study presented already in [Kassianidis et al. 2008] where attention was focused on the particular case of pure azimuthal shear deformation only. In this context, dismissal of either the material incompressibility constraint only or both of the constraints involved in [Soldatos 2009a; 2010] produces two additional versions of the problem. Solution to either of those two versions in the finite strain regime seems to be a more difficult task as compared with the solutions achieved in all three of these references. Nevertheless, the outlined hierarchical manner of approaching difficult problems met in finite elasticity assists enormously the effort of achieving basic understanding of associated complicated issues.

Another plausible way for achieving basic understanding of some of those issues is by restricting initially attention to the small deformation regime within which the material is regarded as linearly elastic. There exists in fact an extensive literature of linear anisotropic elasticity solutions, most of which are associated or can become relevant to the mechanics of fibre-reinforced solids. In this context, the present study adds a new contribution to that literature by focusing attention to the linear elasticity counterpart of each one of the aforementioned four versions of the azimuthal shear strain problem of a transversely isotropic circular cylindrical tube. Based on the outlined history of the problem considered, this investigation aims therefore to identify which of the four versions of the problem anticipate that within the small strain regime (i) existence of possible coupling between azimuthal shear strain and radial stretching can cause change of the inner and outer radii of the tube; and/or (ii) the initial deformation pattern is or may still be interpreted as that of pure azimuthal shear strain, in the sense that the tube inner and outer radii do not tend to changed during deformation. Moreover, (iii) the particular case of straight fibres aligned along the radial direction of the tube cross-section is treated separately and, in the light of the relevant studies initiated in [Soldatos 2009a; 2010], comparisons are made between corresponding solutions and results obtained when fibres are either perfectly flexible or possess bending stiffness.

Under these considerations, section 2 formulates the problem of axially symmetric plane strain of a transversely isotropic, linearly elastic, annular disc (the tube cross-section) subjected to external boundary conditions that may cause pure azimuthal shear strain. It is noted that the formulation detailed in section 2 is based on symmetric elasticity considerations which concur with the assumption that fibres are perfectly flexible. For the case that the direction of transverse isotropy is due to fibres of a certain spiral shape, section 3 outlines next the exact, closed form solution obtained for each one of the aforementioned four versions of the azimuthal shear strain problem; namely, the case in which (i) the material of the tube is completely unconstrained and therefore compressible, (ii) the material is assumed incompressible but the fibres can extent or contract, (iii) the material of the tube is compressible but the fibres are assumed inextensible, and (iv) the material of the tube is incompressible and the fibres are inextensible (ideal fibre-reinforced material). Section 4 deals separately with the particular case of perfectly flexible straight fibres aligned along the radial direction of the tube cross-section. This case, along with its counterpart that considers fibres resistant in bending, was discussed also separately in [Soldatos 2010] for the purposes of the area-preserving finite azimuthal shear strain problem introduced and studied there.

When the perfectly flexible radial fibres considered in section 4 are replaced with radial fibres that posses bending stiffness the linear theory of elasticity is required to account further for possible effects of

couple-stress and therefore asymmetric stress. Moreover, micromechanics considerations reveal that, due to the natural appearance of an intrinsic material length parameter which is of the fibre thickness scale, the manner in which fibres are supported on the tube boundaries can also be accounted for, with use of appropriate boundary conditions. This is the case discussed and resolved completely in section 5, where the principal governing differential equation of the problem is solved exactly with use of the power-series method as well as the successive approximate method introduced in [Soldatos and Hadjigeorgiou 1990]; see also [Shuvalov and Soldatos 2003]. Relevant numerical results are presented in section 6, where the differences between conventional linear elasticity and the new developments introduced in section 5 are also discussed in detail. Finally, section 7 summarises the main results, observations and conclusions drawn in this investigation.

2. Problem formulation for perfectly flexible fibres

Consider a circular cylindrical hollow tube defined by

$$B_0 \le r \le B_1, \qquad 0 \le \theta \le 2\pi, \qquad -\infty \le z \le \infty, \tag{2-1}$$

where r, θ and z are appropriate cylindrical polar coordinate parameters and the nonnegative constants B_0 and B_1 represent the inner and outer radii of the tube, respectively. It is assumed that the tube is made of a transversely isotropic linearly elastic material and that the preferred direction of transverse isotropy lies on the plane of the tube cross-section. Accordingly, the preferred material direction is described as follows (e.g., [Kassianidis et al. 2008]):

$$\theta = G(r) + \theta_0, \qquad G(B_0) = 0, \qquad G(B_1) = \theta_1 - \theta_0 \ge 0, \tag{2-2}$$

where $0 \le \theta_0 \le 2\pi$ and $\theta_1 - \theta_0$ is fixed regardless of the value of θ_0. Here, the scalar function $G(r)$ defines the direction of transverse isotropy which is due to the existence of a single family of plane fibres making an angle $\alpha(r)$ with the radial direction. It is convenient to assume that $0 \le \alpha(r) < \pi/2$ and, hence, that the family of fibres (the a-curves) have the form shown in Figure 1.

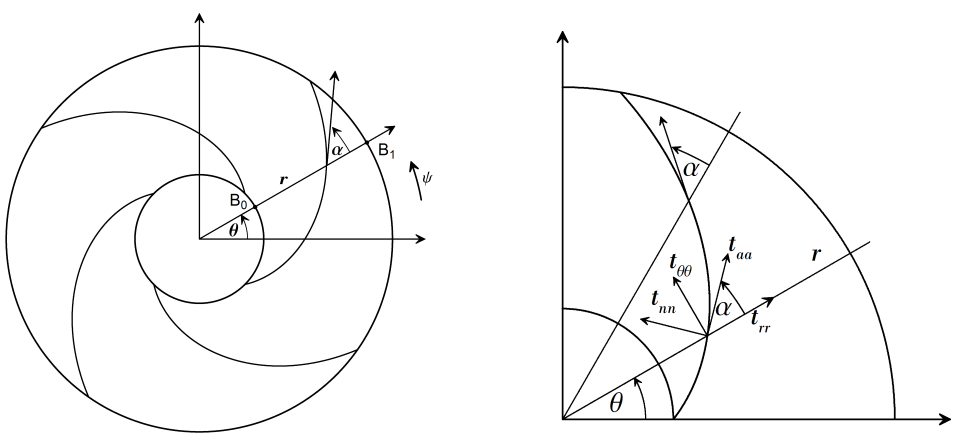

Figure 1. Left: schematic representation of the tube cross-section and associated notation. Right: illustration of normal in-plane stress components in both the local and polar coordinate systems.

The unit tangent $\boldsymbol{a}$ and the unit normal $\boldsymbol{n}$ of this family of material curves form the base of a local rectangular curvilinear coordinate system. In components, these unit vectors are represented as

$$\boldsymbol{a} = (a_r, a_\theta)^T, \qquad \boldsymbol{n} = (-a_\theta, a_r)^T, \tag{2-3}$$

where

$$a_r = \big[(rG'(r))^2 + 1\big]^{-1/2} \qquad a_\theta = rG'(r)\big[(rG'(r))^2 + 1\big]^{-1/2}, \tag{2-4}$$

and a prime denotes differentiation with respect to r. It follows that

$$\tan\alpha = rG'(r), \tag{2-5}$$

and, therefore, $G'(r) \geq 0$.

The material of the tube is assumed to be linearly elastic and, hence, the plane strain version of Hooke's law has the form

$$\begin{pmatrix} t_{aa} \\ t_{nn} \\ t_{an} \end{pmatrix} = \begin{pmatrix} C_{11} & C_{12} & 0 \\ C_{12} & C_{22} & 0 \\ 0 & 0 & C_{66} \end{pmatrix} \begin{pmatrix} e_{aa} \\ e_{nn} \\ 2e_{an} \end{pmatrix}, \qquad t_{zz} = C_{12}e_{aa} + C_{23}e_{nn}, \tag{2-6}$$

where $t_{aa}, t_{nn}, t_{an}, t_{zz}$ and e_{aa}, e_{nn}, e_{an} represent the nonzero components of the stress and the strain tensors respectively, in the aforementioned curvilinear local coordinate system (see also Figure 1, right); $C_{11}, C_{12}, C_{22}, C_{23}$ and C_{66} are appropriate nonzero elastic moduli (e.g., [Jones 1998]) which are assumed constant in what follows. In polar coordinates, $(2\text{-}6)_1$ takes the form

$$\begin{pmatrix} t_{rr} \\ t_{\theta\theta} \\ t_{r\theta} \end{pmatrix} = \begin{pmatrix} \bar{C}_{11} & \bar{C}_{12} & \bar{C}_{16} \\ \bar{C}_{12} & \bar{C}_{22} & \bar{C}_{26} \\ \bar{C}_{16} & \bar{C}_{26} & \bar{C}_{66} \end{pmatrix} \begin{pmatrix} e_{rr} \\ e_{\theta\theta} \\ 2e_{r\theta} \end{pmatrix}, \tag{2-7}$$

where $t_{rr}, t_{\theta\theta}, t_{r\theta}$ and $e_{rr}, e_{\theta\theta}, e_{r\theta}$ are the corresponding polar components of the stress and strain tensors, respectively. In general, it is $\alpha \neq 0$ and, hence, the stiffness matrices $[C]$ and $[\bar{C}]$ appearing in $(2\text{-}6)_1$ and (2-7) are related according to

$$[\bar{C}] = [T]^{-1}[C][T]^{-T}, \tag{2-8}$$

where (e.g., [Jones 1998])

$$[T] = \begin{pmatrix} \cos^2\alpha & \sin^2\alpha & \sin 2\alpha \\ \sin^2\alpha & \cos^2\alpha & -\sin 2\alpha \\ \frac{-1}{2}\sin 2\alpha & \frac{1}{2}\sin 2\alpha & \cos 2\alpha \end{pmatrix}, \tag{2-9}$$

and a superscript $^{-T}$ denotes the inverse of a transposed matrix. It is noted for later use, that both matrices $[C]$ and $[\bar{C}]$ are required to be positive definite, in order for the strain-energy of the system to be positive (e.g., [Ting 1996]).

For the axially symmetric plane deformations of interest, the strain components appearing in (2-7) are

$$e_{rr} = u'(r), \qquad e_{\theta\theta} = \frac{u(r)}{r}, \qquad 2e_{r\theta} = v'(r) - \frac{v(r)}{r}, \tag{2-10}$$

where $u(r)$ and $v(r)$ are the cross-sectional radial and the azimuthal displacement components, respectively. The set of available equations is completed with the equations of equilibrium. In the present case,

these take the form

$$rt'_{rr} + t_{rr} - t_{\theta\theta} = 0, \qquad (r^2 t_{r\theta})' = 0, \qquad \frac{\partial t_{zz}}{\partial z} = 0, \tag{2-11}$$

and, since plane strain assumes that stresses are independent of z, equation (2-11)$_3$ is satisfied identically.

The description of the azimuthal strain problem considered is completed by associating to it appropriate sets of boundary conditions. Accordingly, the boundary conditions imposed in the azimuthal direction of the tube inner and outer boundaries are

$$v(B_0) = 0, \qquad v(B_1) = \psi. \tag{2-12}$$

Since the inner boundary is assumed restrained from rotation, the azimuthal displacement ψ, which is imposed on the tube outer boundary, is assumed to be the cause of the axially symmetric plane-strain deformation of interest. If positive (negative), the known displacement ψ causes an anticlockwise (clockwise) rotation on the outer boundary of the tube cross-section; the azimuthal boundary traction is considered unknown on both boundaries and should therefore be determined from the analysis.

Anticipation of possible coupling between azimuthal shear strain and radial stretching is associated with the ability of the inner and outer tube radii to change during deformation, thus leading to the additional boundary conditions

$$t_{rr}(B_0) = t_{rr}(B_1) = 0. \tag{2-13}$$

However, when pure azimuthal shear strain becomes the principal deformation of interest, the tube radii remain unchanged during deformation and, hence, the natural boundary conditions (2-13) are replaced by the geometrical boundary conditions

$$u(B_0) = u(B_1) = 0. \tag{2-14}$$

3. Spiral fibres

For simplicity, it is now considered that α is constant and, hence, the fibres have the form of a logarithmic spiral; namely, a curve described by the function

$$G(r) = \tan\alpha \ln \frac{r}{B_0}. \tag{3-1}$$

With this relatively simple choice of $G(r)$, the components of the stiffness matrix $[\bar{C}]$ become independent of the polar distance, r. It is seen next that, as a consequence, an exact closed form solution of the problem is possible regardless of whether the material of the tube is unconstrained or is subjected to any combination of the aforementioned incompressibility and inextensibility constrains.

In what follows, equations are made nondimensional with use of the main nondimensional quantities

$$r^* = \frac{r}{B_0}, \qquad \beta = \frac{B_1}{B_0}, \qquad u^* = \frac{u}{\psi}, \qquad v^* = \frac{v}{\psi},$$
$$t^*_{ij} = \frac{B_0 t_{ij}}{\psi \bar{C}_{66}} \quad (i, j = r, \theta), \qquad \bar{C}^*_{ij} = \frac{\bar{C}_{ij}}{\bar{C}_{66}} \quad (i, j = 1, 2, 6). \tag{3-2}$$

It is also noted that the additional nondimensional quantities

$$p^* = \frac{B_0 p}{\psi \bar{C}_{66}}, \qquad T^* = \frac{B_0 T}{\psi \bar{C}_{66}} \tag{3-3}$$

will be employed latter in sections 3.2, 3.3 and 3.4 in order to represent nondimensional forms of the arbitrary pressure and tension, respectively, introduced there. It is however noted that, for convenience, asterisks are dropped in all equations met next in sections 3 and 4. Hence, the form of the in-plane equilibrium equations $(2\text{-}11)_{1,2}$ remains unchanged under the implied nondimensional analysis while the corresponding nondimensional form of the boundary conditions (2-12), (2-13) and (2-14) is, respectively,

$$v(1) = 0, \ v(\beta) = 1, \tag{3-4}$$

$$t_{rr}(1) = t_{rr}(\beta) = 0, \tag{3-5}$$

$$u(1) = u(\beta) = 0. \tag{3-6}$$

3.1. ***Unconstrained material.*** Use of the kinematic equations (2-10) and the Hooke's law (2-7) yields the nondimensional Navier-type form of the equilibrium equations $(2\text{-}11)_{1,2}$ as follows:

$$\begin{aligned} &\bar{C}_{11} r (ru')' - \bar{C}_{22} u + \bar{C}_{16} r^2 v'' - \bar{C}_{26} (rv' - v) = 0, \\ &\bar{C}_{16} (r^2 u')' + \bar{C}_{26} (ru)' + r^2 v'' + rv' - v = 0. \end{aligned} \tag{3-7}$$

This is a system of two second-order simultaneous, Euler-type ordinary differential equations (ODEs) which admit solutions of the form $u(r) = c_1 r^n$, $v(r) = c_2 r^n$.

Accordingly, the general solution of equations (3-7) is found to be

$$\begin{aligned} u(r) &= \gamma_1 \bar{A}_1 r^{-1} + \bar{A}_2 r^{\eta} + \bar{A}_3 r^{-\eta}, \\ v(r) &= \bar{A}_4 r + \bar{A}_1 r^{-1} + \gamma_2 \bar{A}_2 r^{\eta} + \gamma_3 \bar{A}_3 r^{-\eta}, \end{aligned} \tag{3-8}$$

where $\bar{A}_1$, $\bar{A}_2$, $\bar{A}_3$ and $\bar{A}_4$ are arbitrary constants of integration, the constants γ_1, γ_2 and γ_3 are given in the Appendix and

$$\eta^2 = \frac{\bar{C}_{22} - \bar{C}_{26}^2}{\bar{C}_{11} - \bar{C}_{16}^2}. \tag{3-9}$$

It can be shown that, due to the positive definiteness of $[\bar{C}]$, both the numerator and the denominator appearing in the right-hand side of (3-9) are positive and, therefore, η is always a real constant. Use of Hooke's law yields further the associated in-plane nondimensional stress components as follows:

$$\begin{aligned} t_{rr} &= \bar{A}_1 F_1 r^{-2} + \bar{A}_2 F_2 r^{\eta - 1} + \bar{A}_3 F_3 r^{-\eta - 1}, \\ t_{\theta\theta} &= \bar{A}_1 F_4 r^{-2} + \bar{A}_2 F_5 r^{\eta - 1} + \bar{A}_3 F_6 r^{-\eta - 1}, \\ t_{r\theta} &= \bar{A}_1 \left(\gamma_1 (\bar{C}_{26} - \bar{C}_{16}) - 2 \right) r^{-2}, \end{aligned} \tag{3-10}$$

where the constants F_k $(k = 1, 2, \ldots, 6)$ are given explicitly in the Appendix.

The form of the solution (3-8) makes immediately understood that change of both the inner and outer radii of the tube is generally always possible in this case, in which the material of the tube is completely unconstrained. For, if the particular set of boundary conditions (3-4) and (3-5) is considered, all four of

the arbitrary constants appearing in (3-8) and (3-10) acquire the unique nonzero values given explicitly in equations (A-3); hence, $u(r) \neq 0$ for all $1 \leq r \leq \beta$. In this case, the radial displacement of the inner and outer boundary of the tube is determined by setting $r = 1$ and $r = \beta$ in $(3\text{-}8)_1$, respectively.

If, on the other hand, the set of boundary conditions (3-4) and (3-6) is taken instead into consideration, the alternative set of unique nonzero values associated with the aforementioned arbitrary constants — see equations (A-5) — suggests that, although $u(r) \neq 0$ for $1 < r < \beta$ and, therefore, there is coupling between azimuthal shear and radial stretching in the interior of the tube, the boundary radii of the tube can be kept unchanged during deformation. Conditions of pure azimuthal shear can therefore also be observed in this case, although these require simultaneous action of appropriate nonzero normal tractions on the tube inner and outer boundaries; those tractions are determined by setting $r = 1$ and $r = \beta$ in $(3\text{-}10)_1$.

It should be finally noted that in the particular case that $\alpha = 0$ (radial fibres), equations (3-7) become uncoupled and, as a result, azimuthal shear strain and radial stretching become completely uncoupled deformations. It will be seen in what follows that this result is valid regardless of whether the material is constrained or not and, hence, this particular case, in which the fibres are aligned along the radial direction of the tube cross-section, is discussed separately in Section 4.

3.2. ***Incompressible material.*** Incompressibility is a kinematic constraint which requires an arbitrary hydrostatic pressure $p(r)$ to be superimposed on the stress field; $p(r)$ does no work in any deformation which is compatible with the incompressibility constraint ($\operatorname{tr} \boldsymbol{e} = 0$). In this case, Hooke's law (2-7) is modified and its in-plane part takes the nondimensional form (e.g., [Spencer 1972; 1984])

$$\begin{pmatrix} t_{rr} \\ t_{\theta\theta} \\ t_{r\theta} \end{pmatrix} = \begin{pmatrix} \bar{C}_{11} & \bar{C}_{12} & \bar{C}_{16} \\ \bar{C}_{12} & \bar{C}_{22} & \bar{C}_{26} \\ \bar{C}_{16} & \bar{C}_{26} & 1 \end{pmatrix} \begin{pmatrix} e_{rr} \\ e_{\theta\theta} \\ 2e_{r\theta} \end{pmatrix} - p \begin{pmatrix} 1 \\ 1 \\ 0 \end{pmatrix}, \tag{3-11}$$

where, as already mentioned, the appearing quantities are all nondimensionalized according to (3-2) and (3-3) before asterisks are dropped. The nondimensional form of the corresponding Navier-type governing equations then becomes

$$\begin{aligned} &\bar{C}_{11} r (r u')' - \bar{C}_{22} u + \bar{C}_{16} r^2 v'' - \bar{C}_{26} (r v' - v) - r^2 p' = 0, \\ &\bar{C}_{16} (r^2 u')' + \bar{C}_{26} (r u)' + r^2 v'' + r v' - v = 0, \end{aligned} \tag{3-12}$$

and are accompanied by the incompressibility constraint $e_{rr} + e_{\theta\theta} = 0$, which yields the additional equation

$$u' + \frac{u}{r} = 0. \tag{3-13}$$

Solution of (3-13) yields $u(r)$ which is then inserted into $(3\text{-}12)_2$. The latter yields thus an inhomogeneous Euler ODE which is solved in the standard manner for the determination of $v(r)$. Solution of $(3\text{-}12)_1$ becomes next possible for $p(r)$ and, hence, the general solution of the system of simultaneous ODEs (3-12) and (3-13) is found to be

$$u(r) = \tilde{A}_1 r^{-1}, \quad v(r) = \tilde{A}_2 r + \tilde{A}_3 r^{-1}, \quad p(r) = \tilde{A}_4 - \tfrac{1}{2}\big(\tilde{A}_1 (\bar{C}_{11} - \bar{C}_{22}) + 2\tilde{A}_3 (\bar{C}_{16} + \bar{C}_{26})\big) r^{-2}, \tag{3-14}$$

where $\tilde{A}_1$, $\tilde{A}_2$, $\tilde{A}_3$ and $\tilde{A}_4$ are arbitrary constants of integration. Use of the constitutive equation (3-11) yields further the associated in-plane nondimensional stress components:

$$\begin{aligned} t_{rr} &= \big(\tfrac{1}{2}\tilde{A}_1(2\bar{C}_{12} - \bar{C}_{11} - \bar{C}_{22}) + \tilde{A}_3(\bar{C}_{26} - \bar{C}_{16})\big)r^{-2} - \tilde{A}_4, \\ t_{\theta\theta} &= \big(-\tfrac{1}{2}\tilde{A}_1(2\bar{C}_{12} - \bar{C}_{11} - \bar{C}_{22}) - \tilde{A}_3(\bar{C}_{26} - \bar{C}_{16})\big)r^{-2} + \tilde{A}_4, \\ t_{r\theta} &= \big(\tilde{A}_1(\bar{C}_{26} - \bar{C}_{16}) - 2\tilde{A}_3\big)r^{-2}. \end{aligned} \tag{3-15}$$

By considering the particular set of boundary conditions (3-4) and (3-5), $\tilde{A}_1$, $\tilde{A}_2$ and $\tilde{A}_3$ take unique nonzero values — see (A-7) — while $\tilde{A}_4 = 0$. Hence, $u(r) \neq 0$ for all $1 \leq r \leq \beta$ and a change of both the inner and outer radii of the tube is generally again possible in this case. It is also noted that, despite the nonzero values of both $\tilde{A}_1$ and $\tilde{A}_3$, $t_{rr} = t_{\theta\theta} = 0$ throughout the tube cross-section. Finally, if $\alpha = \pi/4$, then $\bar{C}_{16} = \bar{C}_{26}$ and, therefore, $u(r) = 0$ throughout the tube cross-section, thus causing conditions of pure azimuthal shear strain in this particular case.

Conditions of pure azimuthal shear strain are also possible for $\alpha \neq 0$, if only one of the two boundary conditions (3-6) is satisfied along with (3-4). Due to the form of $(3\text{-}14)_1$, the unused of the geometrical boundary conditions (3-6) is satisfied automatically and should therefore be replaced by its natural boundary condition counterpart detailed in (3-5). If, for instance, the set of mixed boundary conditions

$$u(1) = t_{rr}(\beta) = 0, \tag{3-16}$$

is chosen to replace (3-6), while (3-4) still hold, then $\tilde{A}_1 = 0$ and, therefore, $u(r) = 0$ throughout the tube cross-section ($\tilde{A}_2$, $\tilde{A}_3$ and $\tilde{A}_4$ are given by (A-8)). Nevertheless, a nonzero normal traction should act in this case in the radial direction of the tube inner boundary; this is determined by setting $r = 1$ in $(3\text{-}15)_1$. Similar arguments hold true if (3-16) are replaced by $t_{rr}(1) = u(\beta) = 0$. Pure azimuthal shear strain is observed again in this case, though a normal traction should be applied radially on the outer tube boundary.

In the particular case that $\alpha = 0$, equation $(3\text{-}12)_2$ becomes uncoupled from the set of equations $(3\text{-}12)_1$ and (3-13). Hence, azimuthal shear strain and radial stretching become again completely uncoupled deformations. Moreover, since the incompressibility constraint is associated with radial stretching only, the azimuthal strain problem becomes identical with its unconstrained material counterpart; this is the case discussed separately in Section 4.

3.3. ***Inextensible fibres.*** The constraint of fibre inextensibility ($\boldsymbol{a}^T \boldsymbol{e}\boldsymbol{a} = 0$) requires an arbitrary tension $T(r)$ to be superimposed on the stress field; this acts along the fibre direction and does no work in any deformation which conforms with this constraint. In this case Hooke's law takes the nondimensional form (e.g., [Spencer 1972; 1984])

$$\begin{pmatrix} t_{rr} \\ t_{\theta\theta} \\ t_{r\theta} \end{pmatrix} = \begin{pmatrix} \bar{C}_{11} & \bar{C}_{12} & \bar{C}_{16} \\ \bar{C}_{12} & \bar{C}_{22} & \bar{C}_{26} \\ \bar{C}_{16} & \bar{C}_{26} & 1 \end{pmatrix} \begin{pmatrix} e_{rr} \\ e_{\theta\theta} \\ 2e_{r\theta} \end{pmatrix} + T \begin{pmatrix} \cos^2\alpha \\ \sin^2\alpha \\ \sin\alpha\cos\alpha \end{pmatrix}, \tag{3-17}$$

where the appearing quantities are again nondimensionalized according to (3-2) and (3-3) before asterisks are dropped. The nondimensional form of the corresponding Navier-type governing equations then

becomes

$$\bar{C}_{11}r(ru')' - \bar{C}_{22}u + \bar{C}_{16}r^2v'' - \bar{C}_{26}(rv' - v) + r(rT)'\cos^2\alpha - rT\sin^2\alpha = 0,$$
$$\bar{C}_{16}(r^2u')' + \bar{C}_{26}(ru)' + r^2v'' + rv' - v + \tfrac{1}{2}\sin 2\alpha(r^2T)' = 0. \tag{3-18}$$

These are accompanied by the inextensibility constraint $e_{rr}\cot\alpha + e_{\theta\theta}\tan\alpha + 2e_{r\theta} = 0$ which, with use of (2-10), yields the additional equation

$$u'\cot\alpha + \frac{u}{r}\tan\alpha + v' - \frac{v}{r} = 0. \tag{3-19}$$

Equation (3-18)$_2$ can immediately be integrated once. A subsequent elimination of $v(r)$ and $T(r)$ from the resulting equations yields an inhomogeneous second-order Euler-type ODE for $u(r)$ which can be solved in the standard manner. The general solution of the system of simultaneous ODEs (3-18) and (3-19) can then be obtained with relative ease, to yield

$$u(r) = \frac{\hat{A}_1}{\hat{\gamma}_1(1-m^2)}r^{-1} + \hat{A}_2r^m + \hat{A}_3r^{-m},$$
$$v(r) = \hat{A}_4r - \frac{\hat{A}_1\cot 2\alpha}{\hat{\gamma}_1(1-m^2)}r^{-1} - \hat{A}_2\beta_1r^m - \hat{A}_3\beta_2r^{-m},$$
$$T(r) = \frac{2\hat{A}_1}{\sin 2\alpha}\left(1 + \frac{\bar{C}_{16} - \bar{C}_{26} - 2\cot 2\alpha}{\hat{\gamma}_1(1-m^2)}\right)r^{-2}$$
$$+\frac{2\hat{A}_2}{\sin 2\alpha}\left(\beta_1(m-1) - m\bar{C}_{16} - \bar{C}_{26}\right)r^{m-1} + \frac{2\hat{A}_3}{\sin 2\alpha}\left(m\bar{C}_{16} - \beta_2(m+1) - \bar{C}_{26}\right)r^{-m-1}, \tag{3-20}$$

where $\hat{A}_1$, $\hat{A}_2$, $\hat{A}_3$, $\hat{A}_4$ are arbitrary constants of integration, the constants β_1, β_2, $\hat{\gamma}_1$ and $\hat{\gamma}_2$ are given explicitly in the Appendix and

$$m^2 = \frac{\hat{\gamma}_2}{\hat{\gamma}_1}. \tag{3-21}$$

It can be shown that, due to the positive definiteness of the matrix $[C]$ and the fact that $0 \le \alpha < \pi/2$, both the numerator and the denominator in the right-hand side of (3-21) are positive and, therefore, the constant m is always real. Use of (3-17) yields next the associated in-plane nondimensional stress components as follows:

$$t_{rr} = \frac{\hat{A}_1}{\hat{\gamma}_1(1-m^2)}H_1r^{-2} + \hat{A}_2H_2r^{m-1} + \hat{A}_3H_3r^{-m-1},$$
$$t_{\theta\theta} = \frac{\hat{A}_1}{\hat{\gamma}_1(1-m^2)}H_4r^{-2} + \hat{A}_2H_5r^{m-1} + \hat{A}_3H_6r^{-m-1},$$
$$t_{r\theta} = \hat{A}_1r^{-2}, \tag{3-22}$$

where the constants H_k $(k = 1, 2, \ldots, 6)$ are given explicitly in (A-10).

If the set of boundary conditions (3-4) and (3-5) is associated with this solution, all four arbitrary constants appearing in (3-20) and (3-22) take unique nonzero values (see (A-11)); hence, $u(r) \neq 0$ for all $1 \le r \le \beta$. It follows that a solution anticipating that both the inner and the outer tube radii change is again possible in this case. If, on the other hand, the alternative set of boundary conditions

(3-4) and (3-6) is instead considered, the corresponding set of unique nonzero values associated to those constants — see (A-13) — suggests that conditions of pure azimuthal shear strain can instead also be observed. Nevertheless, although the boundary radii of the tube do not change during the observed pure azimuthal shear deformation, it is again $u(r) \neq 0$ for $1 < r < \beta$ and, therefore, there is again coupling between azimuthal shear strain and radial stretching in the interior of the tube. It is again anticipated that appropriate nonzero normal tractions should be applied on the tube inner and outer boundaries; these are determined by setting $r = 1$ and $r = \beta$ in $(3\text{-}22)_1$.

In the case $\alpha = 0$, radial stretching and azimuthal shear strain become again uncoupled deformations. The fibre inextensibility constraint becomes associated with radial stretching in this case, so the azimuthal shear strain problem becomes again identical with its unconstrained material counterpart; see Section 4.

3.4. ***Ideal fibre-reinforced material.*** In this case, the material is assumed to be incompressible and also reinforced by inextensible fibres. Hence, Hooke's law takes the nondimensional form (e.g., [Spencer 1972; 1984])

$$\begin{pmatrix} t_{rr} \\ t_{\theta\theta} \\ t_{r\theta} \end{pmatrix} = \begin{pmatrix} \bar{C}_{11} & \bar{C}_{12} & \bar{C}_{16} \\ \bar{C}_{12} & \bar{C}_{22} & \bar{C}_{26} \\ \bar{C}_{16} & \bar{C}_{26} & 1 \end{pmatrix} \begin{pmatrix} e_{rr} \\ e_{\theta\theta} \\ 2e_{r\theta} \end{pmatrix} + \begin{pmatrix} T\cos^2\alpha - p \\ T\sin^2\alpha - p \\ T\sin\alpha\cos\alpha \end{pmatrix}, \tag{3-23}$$

where the appearing quantities are all nondimensionalized according to (3-2) and (3-3), before asterisks are dropped. The nondimensional form of the corresponding Navier-type governing equations then becomes

$$\begin{aligned} &\bar{C}_{11} r(ru')' - \bar{C}_{22} u + \bar{C}_{16} r^2 v'' - \bar{C}_{26}(rv' - v) + r^2(T'\cos^2\alpha - p') + rT\cos 2\alpha = 0, \\ &\bar{C}_{16}(r^2u')' + \bar{C}_{26}(ru)' + r^2 v'' + rv' - v + \tfrac{1}{2}\sin 2\alpha (r^2 T)' = 0, \end{aligned} \tag{3-24}$$

and are accompanied by both constraint equations (3-13) and (3-19), thus forming a system of four simultaneous ODEs for a total of four unknown functions, namely u, v, p and T.

Solution of Equation (3-13) yields $u(r)$, which is then inserted into (3-19) for the determination of $v(r)$. With the form of $u(r)$ and $v(r)$ becoming thus known, $T(r)$ and $p(r)$ are next obtained by consecutively solving $(3\text{-}24)_2$ and $(3\text{-}24)_1$, respectively. Hence, the general solution of the system of simultaneous ODEs (3-24), (3-13) and (3-19) is found to be

$$\begin{aligned} u(r) &= A_1 r^{-1}, \\ v(r) &= A_2 r - A_1 r^{-1}\cot 2\alpha, \\ p(r) &= A_3 + \tfrac{1}{2}\left(A_4 - A_1(\bar{C}_{11} - \bar{C}_{22} - 2(\bar{C}_{16} + \bar{C}_{26})\cot 2\alpha)\right) r^{-2}, \\ T(r) &= A_4 r^{-2}, \end{aligned} \tag{3-25}$$

where A_1, A_2, A_3, A_4 are arbitrary constants. Use of (3-23) yields next the associated in-plane nondimensional stress components as follows:

$$\begin{aligned} t_{rr} &= \left(\tfrac{1}{2}A_1(2\bar{C}_{12} - \bar{C}_{11} - \bar{C}_{22} + 2(\bar{C}_{16} - \bar{C}_{26})\cot 2\alpha) + \tfrac{1}{2}A_4\cos 2\alpha\right) r^{-2} - A_3, \\ t_{\theta\theta} &= \left(-\tfrac{1}{2}A_1(2\bar{C}_{12} - \bar{C}_{11} - \bar{C}_{22} + 2(\bar{C}_{16} - \bar{C}_{26})\cot 2\alpha) - \tfrac{1}{2}A_4\cos 2\alpha\right) r^{-2} + A_3, \\ t_{r\theta} &= \left(A_1(2\bar{C}_{66} + \bar{C}_{26} - \bar{C}_{16}) + \tfrac{1}{2}A_4\sin 2\alpha\right) r^{-2}. \end{aligned} \tag{3-26}$$

If the solution (3-25) is associated with the set of boundary conditions (3-4) and (3-5), A_1, A_2 and A_4 take unique nonzero values — (A-15) — while $A_3 = 0$. Hence, $u(r) \neq 0$ for all $1 \leq r \leq \beta$ and a change of both the inner and outer radii of the tube is again possible; it is also noted that, despite of the nonzero values of A_1 and A_4, $t_{rr} = t_{\theta\theta} = 0$ throughout the tube cross-section. On the other hand, pure azimuthal shear strain deformation is not possible in this case. For, simultaneous satisfaction of the boundary conditions $(3\text{-}4)_1$ and $(3\text{-}6)_1$ yields $u(r) = v(r) = 0$ throughout the tube cross-section.

It is again seen that in the particular case that $\alpha = 0$, radial stretching and azimuthal shear strain become again uncoupled problems, while both constraints involved associate themselves with radial stretching. Hence, the azimuthal shear strain problem becomes again identical with its unconstrained material counterpart which is discussed in the next section.

4. Perfectly flexible radial fibres

Interest is now focused in the particular case in which the fibres are straight and aligned along the radial direction of the tube cross-section. This corresponds to the choice $G(r) = \alpha = 0$ and, since the local and the polar coordinate systems coincide, the elastic behaviour of the material is described by (2-6), provided that the appearing local in-plane stress and strain components are replaced by their polar counterparts appearing in (2-7). It is already seen that, when $\alpha = 0$, radial stretching and azimuthal shear strain become completely uncoupled deformations regardless of whether the material is constrained or not. Restricting, for instance, attention to the unconstrained material case discussed in Section 3.1, one finds that equations (3-7) become uncoupled when $\alpha = 0$ and, hence, the resulting azimuthal shear strain problem is completely described by the Euler differential equation

$$r^2 v'' + r v' - v = 0. \tag{4-1}$$

This second-order ODE can describe pure azimuthal shear deformation only and, hence, it is associated with the pair of boundary conditions (3-4) only. Solution of this boundary value problem yields

$$v(r) = \frac{\beta}{\beta^2 - 1}\left(r - r^{-1}\right), \tag{4-2}$$

and Hooke's law $(2\text{-}6)_1$ reveals further that the nondimensional azimuthal shear stress

$$t_{r\theta} = \frac{2\beta}{\beta^2 - 1} r^{-2}, \tag{4-3}$$

is the only nonzero stress component associated with this deformation.

Interestingly enough, when the tube material is constrained in the manner suggested in Section 3, every single one of the problems discussed in sections 3.2, 3.3 and 3.4 provides precisely the same description for the pure azimuthal shear strain problem, namely (4-1) and (3-4); hence, in each case, it yields precisely the same solution with the outlined above on the basis of the unconstrained material version of the problem. It also becomes evident that, since material anisotropy does not enter the outlined problem description, the obtained solution (4-2) and (4-3) is identical to its isotropic material counterpart. However, it is already known [Soldatos 2009a; Soldatos 2010] that pure azimuthal shear deformation of a radially reinforced tube made of ideal fibre reinforced material (see Section 3.4) is not possible in the finite deformations regime. In contrast, finite pure azimuthal shear strain is indeed possible if the tube

material is incompressible but the radial fibres involved are free to extend or contract [Kassianidis et al. 2008]. Moreover, the material incompressibility constraint affects in a clear and obvious manner the relevant finite elasticity solution obtained in this latter reference, whereas this fact is not observed in the present case of small deformations (Section 3.2). It is instead observed that conventional linear elasticity theory cannot adequately account for the effects that material anisotropy and/or either of the constraints of material incompressibility and fibre inextensibility have on the azimuthal shear deformation problem considered when the tube is reinforced along the radial direction of its cross-section. In what follows, the infinitesimal strain problem described by (4-1) and (3-4), as well as its relatively simple solution given by (4-2) and (4-3), will therefore be mainly associated with the case discussed in Section 3.1, where the material is assumed completely unconstrained.

5. Radial fibres with bending stiffness

When the perfectly flexible fibres considered in the previous sections are replaced with fibres possessing bending stiffness, the theory is required to account further for possible action of couple-stress and therefore asymmetric stress [Spencer and Soldatos 2007]. The linearized version of the relevant hyper elasticity theory presented in that paper is considered for a study of the effects that fibre bending stiffness has on the azimuthal shear strain problem discussed in the preceding section. For convenience, the restricted part of that linearized theory, which requires use of only one additional elastic modulus, is employed here.

5.1. ***Problem formulation.*** The form of Hooke's law presented in Section 2 for $\alpha = 0$, before the nondimensional quantities (3-2) were introduced, is now suitable only for description of the symmetric part of the stress tensor. Hence,

$$\begin{pmatrix} t_{rr} \\ t_{\theta\theta} \\ t_{(r\theta)} \end{pmatrix} = \begin{pmatrix} C_{11} & C_{12} & 0 \\ C_{12} & C_{22} & 0 \\ 0 & 0 & C_{66} \end{pmatrix} \begin{pmatrix} e_{rr} \\ e_{\theta\theta} \\ 2e_{r\theta} \end{pmatrix}, \tag{5-1}$$

where $t_{(r\theta)}$ denotes the symmetric part of the shear stress component $t_{r\theta}$, the matrix $[C]$ is identical to its counterpart involved in (2-6) and the appearing strain components are given according to (2-10).

The antisymmetric part of $t_{r\theta}$ is caused by the action of a relevant couple-stress component, m_{rz}, arising when fibres resist bending. In terms of a notation similar to that adopted in [Soldatos 2009b], this couple-stress component is given according to

$$m_{rz} = d^f k_\theta^f, \qquad k_\theta^f = v''(r), \tag{5-2}$$

where d^f is the aforementioned additional elastic modulus (fibre bending stiffness) and k_θ^f represents the in-plane curvature component of the fibre in the linear elasticity regime. The antisymmetric part of the shear stress component is then expressed as

$$t_{[\theta r]} = -t_{[r\theta]} = \tfrac{1}{2} m'_{rz} = \tfrac{1}{2} d^f v'''(r). \tag{5-3}$$

It thus becomes immediately understood that radial stretching and azimuthal shear strain remain completely uncoupled deformations regardless of whether the material is constrained or not. Hence, the azimuthal equation of equilibrium $(2\text{-}11)_2$, which is again the only governing equation to be considered,

yields

$$\frac{d^f}{2C_{66}}(r^2v'''' + 2rv''') - (r^2v'' + rv' - v) = 0, \tag{5-4}$$

and makes obvious that the existing material anisotropy is indeed accounted for in this case.

Equation (5-4) is a fourth-order ODE for the azimuthal displacement component $v(r)$ and a unique determination of its solution requires specification of four boundary conditions. Two of them are evidently (2-12) while two more boundary conditions can be deduced from the relevant discussion detailed in [Soldatos 2009b]. Accordingly, the outer boundary ($r = B_1$) is assumed free of couple-stress, thus leading to the additional boundary condition

$$m_{rz}(B_1) = 0, \tag{5-5}$$

while the inner boundary ($r = B_0$) may be assumed either restrained against rotation or free of couple stress. It follows that the last of the four boundary conditions sought is one of the following alternatives:

$$\text{either} \quad v'(B_0) = 0 \quad \text{or} \quad m_{rz}(B_0) = 0. \tag{5-6}$$

It is observed that unlike its perfectly flexible fibres counterpart in (4-1), Equation (5-4) depends on the tube material properties. In this regard, the notation

$$\frac{d^f}{C_{66}} = 2l(B_1 - B_0), \tag{5-7}$$

introduces an intrinsic material length parameter l, which may be considered relevant to the fibre thickness. It is evident that when $l = 0$, (5-4) reduces to its perfectly flexible fibres counterpart. The role of nonzero values of l will become clearer in what follows.

5.2. ***Nondimensional form of governing equations.*** The Navier-type governing differential equation (5-4) and the boundary conditions associated to it are next nondimensionalized with use of the nondimensional quantities introduced in (3-2) and the additional nondimensional parameter

$$\lambda = \frac{l}{B_0} = \frac{d^f}{2C_{66}B_0(B_1 - B_0)}. \tag{5-8}$$

Nevertheless, asterisks are again dropped for convenience and, hence, all relevant quantities appearing without an asterisk in the remaining of this section, as well as Section 6, are those defined in (3-2). Accordingly, with use of (5-2), the nondimensional version of the present boundary value problem is found to be

$$\begin{aligned} &\lambda(\beta - 1)(r^2v'''' + 2rv''') - (r^2v'' + rv' - v) = 0, \\ &v(1) = 0, \quad v(\beta) = 1, \quad v''(\beta) = 0, \end{aligned} \tag{5-9}$$

and

$$\text{either} \quad v'(1) = 0 \quad \text{or} \quad v''(1) = 0. \tag{5-10}$$

It is worth noting that, with simultaneous consideration of $(5\text{-}9)_2$, either condition in (5-10) resembles the boundary condition imposed at the end of an elastic slender beam which is clamped or simply supported, respectively, at $\beta = 1$.

With $l = 0$ in the case of perfectly flexible fibres, the conventional (symmetric) theory of linear elasticity (Sections 2–4) implied that the tube cross-section contains an infinite number of fibres. By associating the intrinsic length parameter l with the fibre thickness, the nonsymmetric stress theory employed in this section implies that the number of fibres as well as their density within the cross-section may be accounted for. Accordingly, if a fibre in the present plane strain case is thought of as a slender rectangle of length $B_1 - B_0$, then its area may be represented by the product $l(B_1 - B_0)$ and, hence, the finite number of fibres, N^f, that can be fitted into the tube cross-section is estimated to be

$$N^f = \frac{2\pi B_0}{l} = \frac{2\pi}{\lambda}. \tag{5-11}$$

It follows that the value of total fibre area is $2\pi B_0(B_1 - B_0)$ and this is independent of the fibre thickness. It is also of interest to note that, by dividing the total fibre area by the tube cross-sectional area, the fibre area fraction is estimated to be

$$S^f = \frac{2B_0}{B_1 + B_0} = \frac{2}{\beta + 1}, \tag{5-12}$$

and depends solely on the value of β. It is, therefore, seen that the value of β is indicative of the density (sparsity) of the fibre distribution within the tube cross-section. This result is illustrated in Table 1, where the total fibre area is calculated as a percentage of the area of the tube cross-section. It is finally noted that (5-11) implies $\lambda \le 2\pi$. With $l \ll B_0$ and, therefore, $\lambda \ll 1$ in many practical applications, this inequality may be perceived as a natural consequence of the fact that thickness of common structural fibres is much smaller than the inner tube radius. However, since B_0 may in principle be smaller than l even if the fibre thickness is of the order of 10μ, values of $\lambda > 1$ are also anticipated by the present theory. In this context, the right-hand-side of (5-8) suggests that different physical interpretations of λ and/or l might also be possible, particularly when $O(\lambda) = 1$.

β	1	1.5	2	2.5	3	4	5	7.5	10	20	50	100
S^f %	100	80	66.7	57.1	50	40	33.3	23.5	18.2	9.5	3.9	2

Table 1. Estimated total area of radial fibres with bending stiffness as a percentage of the area of the tube cross-section.

Solution of the boundary value problem (5-9) and (5-10) is next achieved analytically, via the power series method, and computationally, with use of the successive approximation method (SAM) introduced in [Soldatos and Hadjigeorgiou 1990] (see also [Shuvalov and Soldatos 2003; Ye 2003; Soldatos 2003]).

5.3. ***Power series solution.*** Application of the power series method is based on the following Taylor-type series expansion of the solution sought around $r = 1$:

$$v(r) = \sum_{n=0}^{\infty} a_n (r-1)^n, \tag{5-13}$$

where the constant coefficients a_n $(n = 0, 1, 2, \dots)$ are to be determined. Introduction of (5-13) into $(5\text{-}9)_1$, followed by nullification of the coefficients of like powers of $r-1$, leads to the recurrence

relations

$$a_4 = \frac{a_1 + 2a_2 - 2\lambda(\beta-1)3!a_3}{\lambda(\beta-1)4!},$$

$$a_5 = -\frac{a_0 + 4a_1 + 6a_2 - (6\lambda(\beta-1)+1)3!a_3}{\lambda(\beta-1)5!},$$

$$a_{n+4} = \frac{(n-1)(n+1)!}{\lambda(\beta-1)(n+4)!}a_n + \frac{(2n+1)(n+1)!}{\lambda(\beta-1)(n+4)!}a_{n+1} - \left(\frac{(n+1)!}{(n-1)!} - \frac{1}{\lambda(\beta-1)}\right)\frac{(n+2)!}{(n+4)!}a_{n+2} - \frac{2(n+1)}{(n+4)}a_{n+3}, \quad n \geq 2, \tag{5-14}$$

where a_0, a_1, a_2 and a_3 are arbitrary constants. Use of the boundary conditions (5-9)$_2$ and (5-10)$_1$ yields

$$a_0 = 0, \qquad a_1 = 0, \tag{5-15}$$

while use of (5-9)$_2$ and (5-10)$_2$ yields

$$a_0 = 0, \qquad a_2 = 0. \tag{5-16}$$

In both cases, the values of the remaining constants are then determined numerically with use of the boundary conditions (5-9)$_{3,4}$, after the series expansion (5-13) is truncated to an appropriate number of terms that guarantee convergence of the obtained numerical results to a desired accuracy.

5.4. ***Successive approximation solution.*** Application of the well established successive approximation method introduced in [Soldatos and Hadjigeorgiou 1990] requires initially the conversion of (5-9)$_1$ into a system of four simultaneous first-order linear ODEs. In matrix form, these may be arranged as

$$\{X(r)\}' = [D(r)]\{X(r)\}, \qquad \{X(r)\}^T = \{v, v', v'', v'''\}, \tag{5-17}$$

where the nonzero elements of the matrix $[D(r)]$ are

$$D_{12} = D_{23} = D_{34} = 1, \qquad D_{43} = rD_{42} = -r^2 D_{41} = \frac{1}{\lambda(\beta-1)}, \qquad D_{44} = -\frac{2}{r}. \tag{5-18}$$

For sufficiently thin tubes, an approximate solution is obtained by replacing the variable r appearing in (5-18) with the nondimensional cross-sectional middle-radius parameter $R = (\beta+1)/2$. The resulting approximate system of four simultaneous linear ODEs with constant coefficients may then be written in the form

$$\{X(r)\}' = [D(R)]\{X(r)\}, \tag{5-19}$$

and its general solution can be expressed as follows:

$$\{X(r)\} = [K(r)]\{X(1)\}, \qquad 1 \leq r \leq \beta. \tag{5-20}$$

Here $\{X(1)\}$ denotes the value that the vector $\{X\}$ takes at the inner boundary of the tube, while the elements of the exponential matrix $[K(r)] = \exp[(r-1)D(R)]$ can be evaluated analytically in the manner detailed in [Ye 2003].

If the tube is thick, it is divided in N fictitious, successive and coaxial layers having the same constant thickness, represented by the nondimensional thickness parameter $h = (\beta-1)/N$, and the same material

properties. Upon choosing a suitably large value of N, each individual layer becomes itself a sufficiently thin elastic tube and, as a result, an approximate solution of the form (5-20) is considered satisfactory for the study of its behaviour. The approximate solutions thus obtained for all fictitious layers are then suitably connected by means of appropriate continuity conditions imposed on their fictitious interfaces, thus providing an arbitrarily close solution to that of the exact system (5-17) — see [Shuvalov and Soldatos 2003]. For an illustration of the relevant algorithm, consider the j-th such individual fictitious layer ($j = 1, 2, \ldots, N$), the nondimensional middle-radius parameter of which is given by

$$R^{(j)} = 1 + (h/2)(2j - 1), \tag{5-21}$$

giving thus rise to the exponential matrix

$$[K^{(j)}(r)] = \exp[(r - R^{(j)} + h/2)D(R^{(j)})], \qquad R^{(j)} - h/2 \le r \le R^{(j)} + h/2. \tag{5-22}$$

By requiring continuity of the azimuthal displacement component, the in-plane rotation component and the nonzero components of the stress and couple-stress tensors, one obtains the following continuity conditions on the $N - 1$ fictitious interfaces:

$$\{X^{(j)}(R^{(j)} + h/2)\} = \{X^{(j+1)}(R^{(j+1)} - h/2)\}, \qquad j = 1, 2, \ldots, N - 1. \tag{5-23}$$

Hence, with recursive use of (5-20), (5-22) and (5-23), the solution sought is constructed as follows:

$$\begin{aligned}\{X^{(N)}(R^{(N)} + h/2)\} &= [K^{(N)}(R^{(N)} + h/2)]\{X^{(N-1)}(R^{(N-1)} + h/2)\} \\ &= [K^{(N)}(R^{(N)} + h/2)][K^{(N-1)}(R^{(N-1)} + h/2)]\{X^{(N-2)}(R^{(N-2)} + h/2)\} \\ &= \cdots = [\bar{K}]\{X^{(1)}(R^{(1)} - h/2)\},\end{aligned} \tag{5-24}$$

where

$$[\bar{K}] = \left[\prod_{j=N}^{1} [K^{(j)}(R^{(j)} + h/2)]\right]. \tag{5-25}$$

With further use of the boundary conditions $(5\text{-}9)_{2,3,4}$ and (5-10), Equation (5-24) leads to a linear algebraic system (see [Soldatos and Ye 1995], for example), whose solution yields the distribution of the azimuthal displacement component throughout the tube cross-section. Note that the solution of the problem has been obtained by making use of algebraic manipulations involving 4×4 matrices only.

6. Numerical results and discussion

Equations (4-2) and (4-3) make clear that a convenient way for presentation of numerical results when fibres are perfectly flexible ($\lambda = 0$) is associated with the use of the nondimensional quantities

$$\bar{v}(r) = \frac{\beta^2 - 1}{\beta} v(r) = r - r^{-1}, \qquad \bar{t}_{r\theta}(r) = \frac{\beta^2 - 1}{\beta} t_{r\theta}(r) = 2r^{-2}. \tag{6-1}$$

It is observed that neither of these nondimensional quantities depends on the nondimensional radius parameter β of the tube outer boundary. This observation suggests that both $\bar{v}$ and $\bar{t}_{r\theta}$ maintain the same distribution profile regardless of the tube thickness. This is of course not the case when fibres resist bending but, for convenience in the presentation of numerical results, the azimuthal displacement and

the shear stress distributions predicted in Section 5 are also nondimensionalized further in accordance with (6-1). In this context the additional nondimensional stress parameter

$$\bar{t}_{\theta r} = \frac{\beta^2 - 1}{\beta}\, t_{\theta r}$$

is also employed where necessary. It should be emphasized that the profiles of the nondimensional displacement and stress distributions employed do depend on β when fibres resist bending. For a straightforward interpretation of the presented numerical results, it is convenient to assume that $\psi > 0$ and, hence, that the cause of the deformation is applied anticlockwise on the outer tube boundary.

Most of the numerical results shown next are related with relatively thick tubes and they are mainly produced by solving equation $(5\text{-}9)_1$ on the basis of the SAM outlined in Section 5.4. It is worth noting that corresponding numerical results obtained on the basis of the power series method (Section 5.3) are practically identical to those based on SAM and, hence, in line with the conclusions made in [Shuvalov and Soldatos 2003], the two methods are found to be computationally equivalent. However, due mainly to its slow convergence, the power series method seems to be computationally reliable for relatively thin tubes only. In contrast, SAM converges faster and is computationally reliable for a much wider range of the tube thicknesses. Very satisfactory convergence of SAM and accuracy of the obtained results was achieved by choosing $h/R^{(j)} < 0.01$ where h and $R^{(j)}$ are defined in Section 5.4; this fact is also in agreement with similar observations made in previous studies that were based on SAM (e.g., [Soldatos and Ye 1995]). It is convenient at this point to also note that numerical results shown in Figures 2–5 are obtained under the assumption that the geometric boundary condition $(5\text{-}10)_1$ is applied at the fibre root, $r = 1$, while corresponding results plotted in Figures 6-8 are obtained by assuming that the natural boundary condition $(5\text{-}10)_2$ is applied there.

Figure 2 depicts the first quadrant of the tube cross-section and, for different values of λ, shows the deformation pattern of a fibre initially aligned along the horizontal radius of the tube cross-section having its outer boundary at $\beta = 2.5$. It is recalled that $\lambda = 0$ represents the deformation pattern of a perfectly

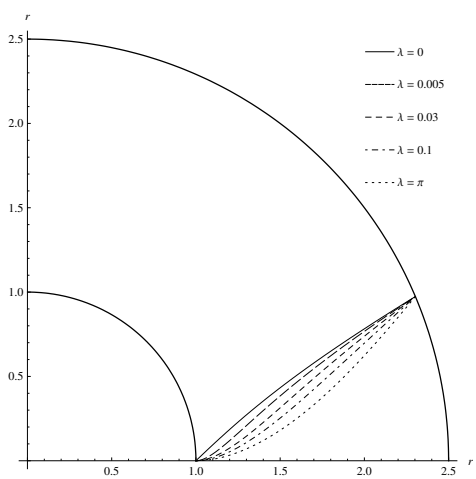

Figure 2. Deformation pattern of a fibre initially aligned along the horizontal radius of the tube cross-section. The fibre is assumed clamped in the inner tube boundary.

flexible fibre described by (4-2). As already mentioned, this pattern is identical to that attained by the horizontal radius of a corresponding isotropic material; having no bending stiffness, a perfectly flexible radial fibre just seems to follow passively the deformation pattern of an isotropic material. Corresponding deformation patterns for a fibre that resists bending ($\lambda \neq 0$) are plotted in Figure 2 under the assumption that the additional boundary condition $(5\text{-}10)_1$ is applied on the tube inner boundary; hence, the fibre is essentially assumed clamped there. It is observed that the slope of the perfectly flexible fibre is nonzero at the inner boundary of the tube cross-section and is monotonically decreasing with increasing β. Hence, a deformed perfectly flexible fibre is concave downwards. In contrast, in their deformed configuration, fibres with bending stiffness are initially concave upwards and, hence, they resist the applied azimuthal shear deformation. This resistance increases with λ and reflects on the slope of the deformed fibre which is initially increasing from its zero value imposed on the inner tube boundary. Although the slope of the fibre begins afterwards to decrease again when λ is small, the region of monotonically increasing slope values becomes larger with increasing λ and, therefore, with increasing fibre bending resistance, in line with physical expectation. For sufficiently large values of λ, the slope of the fibre deformation pattern seems to become monotonically increasing throughout the tube cross-section ($1 \leq r \leq 2.5$) and, hence, the whole fibre is concave upwards. It is finally noted that the deformed fibre pattern shown in Figure 2 for $\lambda = \pi$ remains practically unchanged if λ is increased further.

The dimensionless azimuthal displacement $\bar{v}$ is plotted in Figure 3 against r, for different values of β and for $\lambda = 0.1$. As already mentioned, in the perfectly flexible fibres case ($\lambda = 0$), $\bar{v}$ maintains the same distribution profile regardless of the value of β. However, each one of the dashed lines ($\lambda \neq 0$) begins at the tube inner boundary, as required by the boundary condition $(5\text{-}9)_2$, and ends at some different point of the solid line; namely, at the point β where the external azimuthal displacement ψ is applied on. It is seen that, for $\lambda \neq 0$, $\bar{v}$ is decreasing at the vicinity of the tube inner boundary with increasing β. This is in line with the expectation that, upon increasing the tube outer radius, the effect of the external cause of the deformation is decreasing at the root of the clamped fibre where the highest bending resistance is observed.

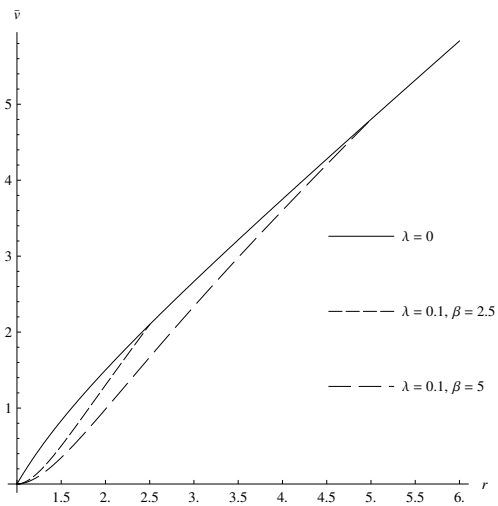

Figure 3. Nondimensional displacement $\bar{v}$ as a function of r for different values of β ($\lambda = 0.1$).

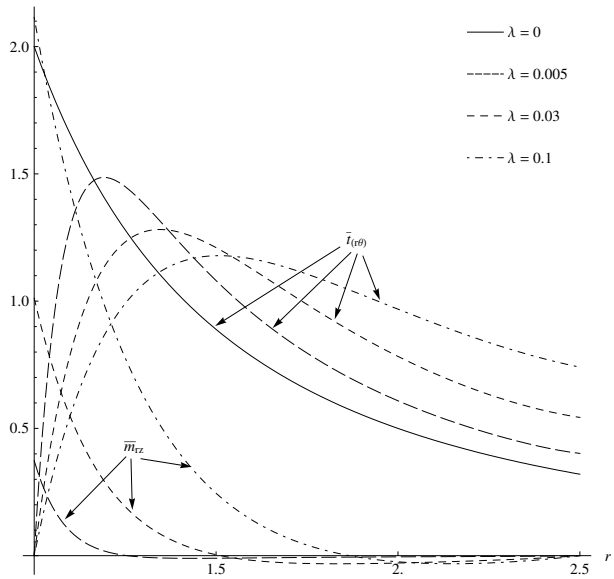

Figure 4. Symmetric part of nondimensional shear stress $\bar{t}_{(r\theta)}$ and nondimensional couple stress $\bar{m}_{rz} = \frac{\beta^2-1}{\beta\psi C_{66}} m_{rz}$ as a function of r for different values of λ ($\beta = 2.5$).

For different values of λ and for $\beta = 2.5$, Figure 4 shows the variation of the symmetric part of the nondimensional shear stress $\bar{t}_{r\theta}$ and the nondimensional couple-stress $\bar{m}_{rz}$ against r. It is recalled that $\bar{t}_{r\theta} = \bar{t}_{\theta r}$ for the perfectly flexible fibre case ($\lambda = 0$); this fact is represented by the solid line in the figure. As a result of the displacement boundary conditions $(5\text{-}9)_2$ and $(5\text{-}10)_1$, $\bar{t}_{(r\theta)}$ is zero at the inner tube boundary; see also (5-1). It follows that the couple-stress $\bar{m}_{rz}$ and, therefore, the antisymmetric part of the shear stress, $\bar{t}_{[r\theta]}$, are dominant at the vicinity of the inner tube boundary; in fact the couple-stress takes naturally its maximum value at the inner tube boundary where highest fibre bending resistance is observed. However, as distance from the inner tube boundary is increasing, the contribution of $\bar{t}_{(r\theta)}$ is increasing while that of $\bar{m}_{rz}$ and $\bar{t}_{[r\theta]}$ is decreasing fast and becomes gradually negligible. As λ increases, $\bar{t}_{(r\theta)}$ decreases within the inner part of the tube cross-section. This decrease of $\bar{t}_{(r\theta)}$ is compensated by the increasing contribution of $\bar{m}_{rz}$ while the outlined trend is reversed within the outer part of the tube cross-section.

For different values of λ and for $\beta = 2.5$, Figure 5, top, shows the distribution of the shear stresses $\bar{t}_{r\theta}$ and $\bar{t}_{\theta r}$ within the tube cross-section. It is seen that, maximum absolute shear stress occurs always at the inner tube boundary, though $\bar{t}_{r\theta}$ and $\bar{t}_{\theta r}$ take opposite values there for $\lambda \neq 0$; this is due to the fact that $\bar{t}_{(r\theta)} = 0$ at $r = 1$, as observed in Figure 4. The absolute value of maximum shear stress increases with increasing the value of λ but, away from the fibre root, $\bar{t}_{r\theta}$ decreases gradually from its maximum positive value while $\bar{t}_{\theta r}$ increases sharply from its corresponding negative minimum value. This is due to the fact that fibre bending resistance has not a dominant effect away from the inner tube boundary. Hence, the stress tensor becomes nearly symmetric outside a certain layer in the vicinity of the inner tube boundary, where negative $\bar{t}_{\theta r}$ values of large magnitude are observed; the width of that layer is naturally increasing with increasing the fibre bending stiffness. For different values of β and for $\lambda = 0.1$, Figure 5, bottom, shows the distribution of $\bar{t}_{r\theta}$ and $\bar{t}_{\theta r}$ within the tube cross-section. As already mentioned, $\bar{t}_{r\theta}$ maintains

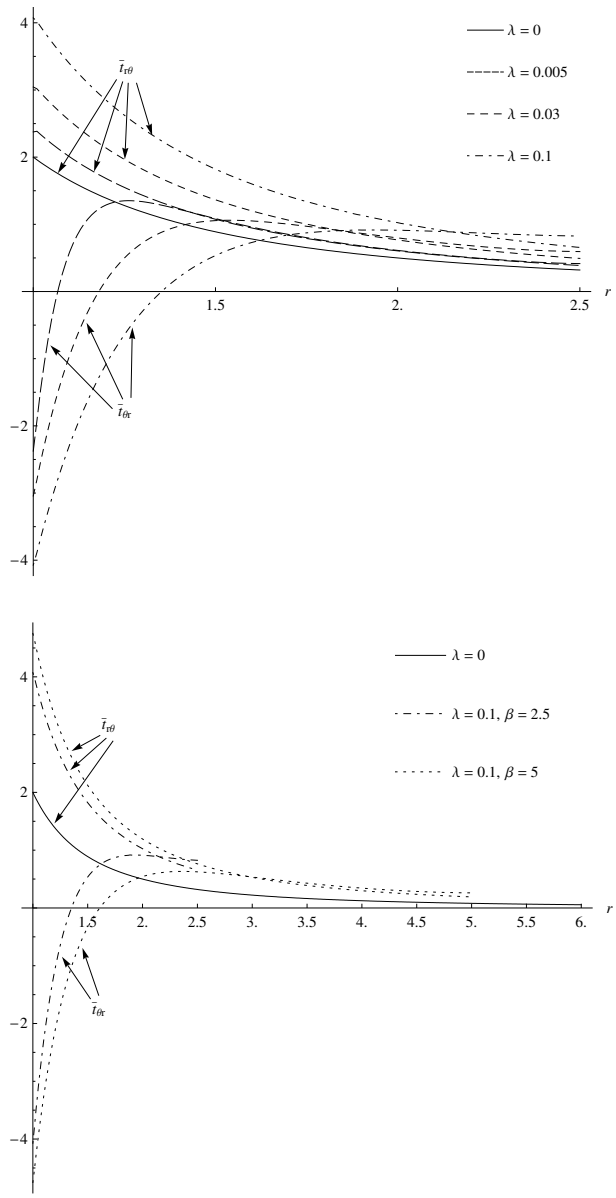

Figure 5. Distribution of shear stresses $\bar{t}_{r\theta}$ and $\bar{t}_{\theta r}$ for $\beta = 2.5$ and different values of λ (top), and for $\lambda = 0.1$ and different values of β (bottom).

again the same distribution profile in the perfectly flexible fibres case (solid line) regardless of the value of β. The figure shows that, when fibres resist bending ($\lambda \neq 0$), $\bar{t}_{r\theta}$ is increasing while $\bar{t}_{\theta r}$ is decreasing near the tube inner boundary with increasing β. It is observed that, the thicker is the tube the nearer the dashed lines approach the solid line at the outer tube boundary. Hence, for sufficiently thick tubes, the effects of fibre bending resistance are essentially confined within the aforementioned layer formed in the neighbourhood of the inner tube boundary; they are not felt in the vicinity of the outer tube boundary.

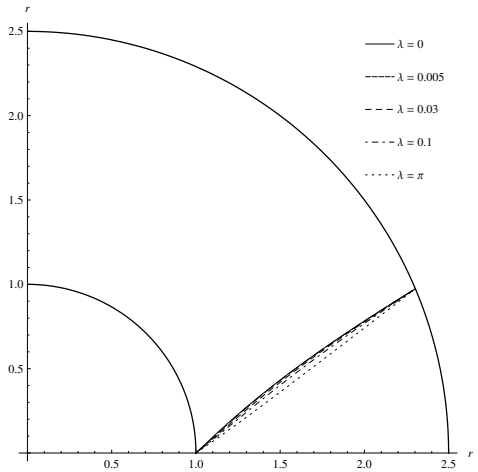

Figure 6. Deformation pattern of a fibre initially aligned along the horizontal radius of the tube cross-section; the fibre is assumed simply supported in the inner tube boundary.

When the geometrical boundary condition $(5\text{-}10)_1$ is replaced by the natural boundary condition $(5\text{-}10)_2$, the numerical values and the physical trends of the results plotted in Figures 2, 4 and 5, top, change dramatically and transform into those depicted in Figures 6, 7 and 8, respectively. Since the root of the fibre is essentially subjected to a simply supported type of boundary condition, the slope of the fibre is nonzero at $r = 1$; see Figure 6. However, the fibre still exhibits signs of bending resistance which, according to Figure 7, seem to emerge slightly further away from the fibre root, as soon as nonzero values of $\bar{m}_{rz}$ become influential. Nevertheless, the total bending resistance of the fibre influences considerably

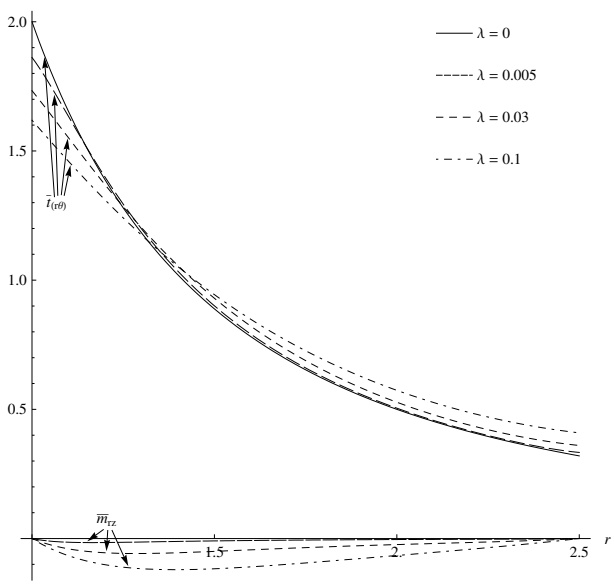

Figure 7. Symmetric part of nondimensional shear stress $\bar{t}_{(r\theta)}$ and nondimensional couple stress $\bar{m}_{rz} = \frac{\beta^2-1}{\beta\psi C_{66}} m_{rz}$ as a function of r for different values of λ ($\beta = 2.5$).

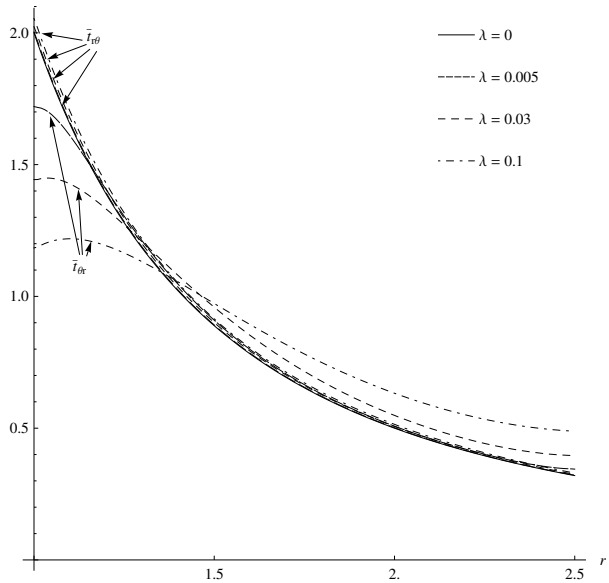

Figure 8. Distribution of shear stresses $\bar{t}_{r\theta}$ and $\bar{t}_{\theta r}$ for different values of λ ($\beta = 2.5$).

the value of the fibre slope at $r = 1$; see Table 2. As a result, the main difference between the values of $\bar{t}_{r\theta}$ and $\bar{t}_{\theta r}$ is again confined within the aforementioned layer near the inner tube boundary (Figure 8). It is also seen (Figure 6) that the maximum possible deviation of the deformed fibre from the deformed shape of its perfectly flexible counterpart is now naturally smaller than that observed in Figure 2.

λ	0	0.005	0.03	0.1	π
$v'(1)$	0.952	0.887	0.825	0.771	0.674

Table 2. The value of the boundary slope of a fibre supported according to $(5\text{-}10)_2$.

It is worth observing in this regard that for large values of λ (e.g., $\lambda = \pi$ in Figure 6) the shape of the deformed fibre is approximately still that of a straight line (that shape remains practically unchanged if the value of λ is increased further). A connection is therefore made between this observation and a conclusion drawn in [Soldatos 2009a; 2010], according to which, in the case of an ideal fibre-reinforced material, the inextensible radial fibres involved do not bend during azimuthal shear deformation; instead they remain straight during deformation and they force the tube cross-section to undergo area-preserving azimuthal shear strain, by changing their slope only. Nevertheless, small area-preserving and small pure azimuthal shear strain are essentially identical deformations in the present case of interest. Hence, radial fibres possessing high bending resistance ($\lambda \geq \pi$) appear to remain practically straight during deformation but they also extend in a manner that satisfies the conditions of pure azimuthal shear strain. If the fibres were inextensible, they would necessarily force the inner and outer tube boundaries to move, as observed in those same references, where the tube material was also assumed to be incompressible. However, as already mentioned, linear elasticity cannot adequately account for the effects that the constraints, of material incompressibility and/or fibre inextensibility have on the azimuthal shear deformation when the

tube is reinforced along the radial direction of its cross-section. In this regard, recall that the relevant area preserving azimuthal shear deformation observed in [Soldatos 2009a; 2010] for ideal fibre-reinforced materials takes place only in the finite elastic deformation regime.

7. Closure

In dealing with the principal questions addressed in the Introduction, it has been found that, when spiral fibres are perfectly flexible, both the inner and the outer radii of the tube exhibit a change for all four versions of the azimuthal shear strain problem considered in Section 3; this change is caused by the existence of coupling between azimuthal shear strain and radial stretching. Nevertheless, it has been also observed that conditions of pure azimuthal shear are possible in all but one of the cases considered and studied in Section 3, though different relevant conditions and/or requirements may apply to different versions of the problem. The only version of the problem for which small pure azimuthal shear strain is not possible is that of the ideal fibre-reinforced material discussed in Section 3.4. This result is in complete agreement with the relevant conclusion made in [Soldatos 2009a; 2010] according which, a tube made from an ideal fibre-reinforced material should instead be expected to undergo area preserving azimuthal shear strain. It is however also noted that area preserving azimuthal shear strain for ideal fibre-reinforced materials [Soldatos 2009a; 2010] is possible only within the finite elastic deformation regime.

When the fibres are straight and aligned along the radial direction of the tube cross-section, radial stretching and azimuthal shear strain become completely uncoupled deformations regardless of whether the tube material is constrained or not, and regardless of whether fibres are perfectly flexible or resist bending. In the perfectly flexible fibres case, the description and, hence, the solution of the problem becomes identical to that met in isotropic elasticity. It is therefore observed that conventional linear elasticity theory cannot adequately account for the effects that the material anisotropy and/or either of the constraints of material incompressibility and fibre inextensibility have on the azimuthal shear strain problem considered when the tube is reinforced along the radial direction of its cross-section.

On the other hand, effects of material anisotropy can be accounted for when fibres posses bending stiffness, by taking into consideration the action of couple-stress and therefore asymmetric stress. It is also seen that the natural appearance of an intrinsic material length parameter, which is representative of the fibre thickness, provides ability for consideration of the manner in which the fibres are supported on the tube boundaries. Hence, when the fibres are assumed clamped in the tube inner boundary, considerable fibre bending resistance is observed within a certain layer in the neighbourhood of the inner tube boundary; there, the fibres appear concave against the imposed deformation, which is in line with physical expectations. It is also observed that the absolute maximum values of the couple-stress and the shear stresses occur at the inner tube boundary where highest bending resistance is anticipated; these values stay influential within the aforementioned layer near the inner tube boundary. When the fibres are assumed simply supported at the inner tube boundary, their slope is naturally nonzero there. However, the fibres still exhibit bending resistance which emerges slightly further away from the fibre root, as soon as nonzero values of the couple-stress become influential. It is also seen that the maximum possible deviation of the deformed simply supported fibre from the deformed shape of its perfectly flexible counterpart is naturally smaller than that observed in the clamped fibre case.

It is also observed that, for large values of fibre bending stiffness, the deformed simply supported radial fibre remains approximately straight. This observation is in line with a conclusion drawn in [Soldatos 2009a; 2010] according to which, in the case of an ideal fibre-reinforced material, the inextensible radial fibres involved do not bend during azimuthal shear deformation; instead they remain straight during deformation and they force the tube cross-section to undergo area-preserving azimuthal shear strain by changing their slope only. Nevertheless, small area-preserving and small pure azimuthal shear strain are essentially identical deformations. Hence, radial fibres possessing high bending resistance appear to remain practically straight during deformation but they also extend in a manner that satisfies the conditions of pure azimuthal shear strain. If the fibres were inextensible, they would necessarily force the inner and outer tube boundaries to move, as observed in [Soldatos 2009a; 2010], where the tube material was also assumed to be incompressible.

Appendix: Explicit form of auxiliary parameters and formulas

The constants γ_1, γ_2 and γ_3 appearing in (3-8) are as follows:

$$\gamma_1 = \frac{2(\bar{C}_{16}+\bar{C}_{26})}{\bar{C}_{22}-\bar{C}_{11}}, \qquad \gamma_2 = -\frac{(\eta\bar{C}_{16}+\bar{C}_{26})}{\eta-1}, \qquad \gamma_3 = -\frac{(\eta\bar{C}_{16}-\bar{C}_{26})}{\eta+1}. \tag{A-1}$$

The constants F_k $(k = 1, 2, \ldots, 6)$ appearing in (3-10) are as follows:

$$\begin{aligned} F_1 &= \gamma_1(\bar{C}_{12}-\bar{C}_{11})-2\bar{C}_{16}, & F_4 &= \gamma_1(\bar{C}_{22}-\bar{C}_{12})-2\bar{C}_{26},\\ F_2 &= \bar{C}_{12}+\eta\bar{C}_{11}+\gamma_2\bar{C}_{16}(\eta-1), & F_5 &= \bar{C}_{22}+\eta\bar{C}_{12}+\gamma_2\bar{C}_{26}(\eta-1),\\ F_3 &= \bar{C}_{12}-\eta\bar{C}_{11}-\gamma_3\bar{C}_{16}(\eta+1), & F_6 &= \bar{C}_{22}-\eta\bar{C}_{12}-\gamma_3\bar{C}_{26}(\eta+1). \end{aligned} \tag{A-2}$$

For the set of boundary conditions (3-4) and (3-5), the arbitrary nonzero constants appearing in (3-8) are found to be

$$\begin{aligned} \bar{A}_1 &= \frac{\beta F_2F_3(\beta^{2\eta}-1)}{\bar{A}}, \qquad \bar{A}_2 = \frac{\beta F_1F_3(\beta^{\eta-1}-1)}{\bar{A}}, \qquad \bar{A}_3 = \frac{-\beta^{\eta}F_1F_2(\beta^{\eta+1}-1)}{\bar{A}},\\ \bar{A}_4 &= \frac{\beta F_3(F_2-\gamma_2F_1)-\beta^{2\eta+1}F_2(F_3-\gamma_3F_1)+\beta^{\eta}F_1(\gamma_2F_3-\gamma_3F_2)}{\bar{A}}, \end{aligned} \tag{A-3}$$

where

$$\bar{A} = \beta^2F_3(F_2-\gamma_2F_1)(\beta^{2\eta-2}+1)-F_2(F_3-\gamma_3F_1)(\beta^{2\eta+2}+1)+2\beta^{\eta+1}F_1(\gamma_2F_3-\gamma_3F_2). \tag{A-4}$$

For the set of boundary conditions (3-4) and (3-6), the corresponding nonzero constants are found to be

$$\begin{aligned} \bar{A}_1 &= \frac{-\beta(\beta^{2\eta}-1)}{\bar{A}}, \qquad \bar{A}_2 = \frac{\gamma_1\beta(\beta^{\eta-1}-1)}{\bar{A}}, \qquad \bar{A}_3 = \frac{\beta^{\eta}(\beta^{\eta+1}-1)}{\bar{A}},\\ \bar{A}_4 &= \frac{\beta(\gamma_1\gamma_2-1)-\beta^{\eta}\gamma_1(\gamma_2-\gamma_3)+\beta^{2\eta+1}(1-\gamma_1\gamma_3)}{\bar{A}}, \end{aligned} \tag{A-5}$$

where

$$\bar{A} = \beta^2\gamma_1\gamma_2(\beta^{\eta-1}-1)^2-\gamma_1\gamma_3(\beta^{\eta+1}-1)^2+(\beta^2-1)(\beta^{2\eta}-1). \tag{A-6}$$

For the set of boundary conditions (3-4) and (3-5), the arbitrary constants appearing in (3-14) are found to be

$$\tilde{A}_1 = \frac{2\beta(\bar{C}_{16} - \bar{C}_{26})}{(\beta^2-1)(\bar{C}_{11} + \bar{C}_{22} - 2\bar{C}_{12})}, \qquad \tilde{A}_2 = \frac{\beta}{\beta^2-1}, \qquad \tilde{A}_3 = \frac{-\beta}{\beta^2-1}. \tag{A-7}$$

For the set of the boundary conditions (3-4) and (3-16), these constants are found to be

$$\tilde{A}_2 = \frac{\beta}{\beta^2-1}, \qquad \tilde{A}_3 = \frac{-\beta}{\beta^2-1}, \qquad \tilde{A}_4 = \frac{\bar{C}_{16} - \bar{C}_{26}}{\beta(\beta^2-1)}. \tag{A-8}$$

The constants β_1, β_2, $\hat{\gamma}_1$ and $\hat{\gamma}_2$ appearing in (3-20) are as follows:

$$\begin{aligned}
\beta_1 &= \frac{m\cot\alpha + \tan\alpha}{m-1}, \qquad \beta_2 = \frac{m\cot\alpha - \tan\alpha}{m+1}, \\
\hat{\gamma}_1 &= \frac{C_{22}}{2}\sin 2\alpha + \frac{\cos^3\alpha}{\sin\alpha}(\cos^4\alpha + \sin^4\alpha), \\
\hat{\gamma}_2 &= \frac{C_{22}}{2}\sin 2\alpha + \frac{\sin^3\alpha}{\cos\alpha}(\cos^4\alpha + \sin^4\alpha).
\end{aligned} \tag{A-9}$$

The constants H_k $(k = 1, 2, \ldots, 6)$ appearing in (3-22) are as follows:

$$\begin{aligned}
H_1 &= \bar{C}_{12} - \bar{C}_{11} + 2\bar{C}_{16}\cot 2\alpha + \cot\alpha\left(\bar{C}_{16} - \bar{C}_{26} - 2\cot 2\alpha + \hat{\gamma}_1(1-m^2)\right), \\
H_2 &= m\bar{C}_{11} + \bar{C}_{12} - \bar{C}_{16}\beta_1(m-1) + m\cot^2\alpha + 1 - \cot\alpha(m\bar{C}_{16} + \bar{C}_{26}), \\
H_3 &= \bar{C}_{12} - m\bar{C}_{11} + \bar{C}_{16}\beta_2(m+1) + 1 - m\cot^2\alpha + \cot\alpha(m\bar{C}_{16} - \bar{C}_{26}), \\
H_4 &= \bar{C}_{22} - \bar{C}_{12} + 2\bar{C}_{26}\cot 2\alpha + \tan\alpha\left(\bar{C}_{16} - \bar{C}_{26} - 2\cot 2\alpha + \hat{\gamma}_1(1-m^2)\right), \\
H_5 &= m\bar{C}_{12} + \bar{C}_{22} - \bar{C}_{26}\beta_1(m-1) + m + \tan^2\alpha - \tan\alpha(m\bar{C}_{16} + \bar{C}_{26}), \\
H_6 &= \bar{C}_{22} - m\bar{C}_{12} + \bar{C}_{26}\beta_2(m+1) + \tan^2\alpha - m + \tan\alpha(m\bar{C}_{16} - \bar{C}_{26}).
\end{aligned} \tag{A-10}$$

For the set of boundary conditions (3-4) and (3-5), the arbitrary constants appearing in (3-20) are found to be

$$\begin{aligned}
\hat{A}_1 &= \frac{\beta\hat{\gamma}_1 H_2 H_3(1-m^2)(\beta^{2m}-1)}{\hat{A}}, \\
\hat{A}_2 &= \frac{-\beta H_1 H_3(\beta^{m-1}-1)}{\hat{A}}, \qquad \hat{A}_3 = \frac{-\beta^m H_1 H_2(\beta^{m+1}-1)}{\hat{A}}, \\
\hat{A}_4 &= \frac{\beta\left(H_2 H_3(\beta^{2m}-1)\cot 2\alpha - \beta^{m-1}H_1(H_3\beta_1 - H_2\beta_2) - H_1(\beta^{2m}H_2\beta_2 - H_3\beta_1)\right)}{\hat{A}},
\end{aligned} \tag{A-11}$$

where

$$\begin{aligned}
\hat{A} = {} & H_1(\beta^{2m}H_3\beta_1 - H_2\beta_2) + H_2H_3(\beta^2-1)(\beta^{2m}-1)\cot 2\alpha \\
& - \beta^2\left(2\beta^{m-1}H_1(H_3\beta_1 - H_2\beta_2) + H_1(\beta^{2m}H_2\beta_2 - H_3\beta_1)\right).
\end{aligned} \tag{A-12}$$

For the set of boundary conditions (3-4) and (3-6), these constants are found to be

$$\hat{A}_1 = \frac{\beta\hat{\gamma}_1(1-m^2)(\beta^{2m}-1)}{\hat{A}}, \qquad \hat{A}_2 = \frac{-\beta(\beta^{m-1}-1)}{\hat{A}}, \qquad \hat{A}_3 = \frac{-\beta^m(\beta^{m+1}-1)}{\hat{A}},$$
$$\hat{A}_4 = \frac{\beta^m(\beta_1-\beta_2)-\beta(\beta_1-\cot 2\alpha)+\beta^{2m+1}(\beta_2-\cot 2\alpha)}{\hat{A}}, \tag{A-13}$$

where

$$\hat{A} = \beta_1\beta^2(\beta^{m-1}-1)^2 - \beta_2(\beta^{m+1}-1)^2 + (\beta^2-1)(\beta^{2m}-1)\cot 2\alpha. \tag{A-14}$$

For the set of boundary conditions (3-4) and (3-5), the arbitrary nonzero constants appearing in (3-25) are found to be

$$A_1 = \frac{\beta\tan 2\alpha}{\beta^2-1}, \qquad A_2 = \frac{\beta}{\beta^2-1},$$
$$A_4 = \frac{\beta\sec 2\alpha\tan 2\alpha}{\beta^2-1}\left(\bar{C}_{11}+\bar{C}_{22}-2\bar{C}_{12}-2(\bar{C}_{16}-\bar{C}_{26})\cot 2\alpha\right). \tag{A-15}$$

References

[Dorfmann et al. 2010] A. Dorfmann, J. Merodio, and R. W. Ogden, "Non-smooth solutions in the azimuthal shear of an anisotropic nonlinearly elastic material", *J. Eng. Math.* **68**:1 (2010), 27–36.

[Jones 1998] R. M. Jones, *Mechanics of composite materials*, Taylor & Francis, 1998.

[Kassianidis et al. 2008] F. Kassianidis, R. W. Ogden, J. Merodio, and T. J. Pence, "Azimuthal shear of a transversely isotropic elastic solid", *Math. Mech. Solids* **13**:8 (2008), 690–724.

[Rivlin 1949] R. S. Rivlin, "Large elastic deformations of isotropic materials, VI: further results in the theory of torsion, shear and flexure", *Philos. Tr. R. Soc. S. A* **242**:845 (1949), 173–195.

[Shuvalov and Soldatos 2003] A. L. Shuvalov and K. P. Soldatos, "On the successive approximation method for three-dimensional analysis of radially inhomogeneous tubes with an arbitrary cylindrical anisotropy", *J. Sound Vib.* **259**:1 (2003), 233–239.

[Soldatos 2003] K. P. Soldatos, "Accurate stress analysis of laminated composite structures", pp. 69–132 in *Modern trends in composite laminates mechanics*, edited by H. Altenbach and W. Becker, Courses and lectures / International Centre for Mechanical Sciences **448**, Springer, 2003.

[Soldatos 2009a] K. Soldatos, "Azimuthal shear deformation of an ideal fibre-reinforced tube according to a second gradient hyper-elasticity theory", session GS–CM – Continuum Mechanics, ID 0017 in *Proc. 7th EUROMECH Solid Mech. Conf.* (Lisbon, 2009), edited by J. Ambrósio et al., 2009.

[Soldatos 2009b] K. P. Soldatos, "Towards a new generation of 2D mathematical models in the mechanics of thin-walled fibre-reinforced structural components", *Int. J. Eng. Sci.* **47**:11-12 (2009), 1346–1356.

[Soldatos 2010] K. Soldatos, "Second-gradient plane deformations of ideal fibre-reinforced materials: implications of hyper-elasticity theory", *J. Eng. Math.* **68**:1 (2010), 99–127.

[Soldatos and Hadjigeorgiou 1990] K. P. Soldatos and V. P. Hadjigeorgiou, "Three-dimensional solution of the free vibration problem of homogeneous isotropic cylindrical shells and panels", *J. Sound Vib.* **137**:3 (1990), 369–384.

[Soldatos and Ye 1995] K. P. Soldatos and J. Q. Ye, "Axisymmetric static and dynamic analysis of laminated hollow cylinders composed of monoclinic elastic layers", *J. Sound Vib.* **184**:2 (1995), 245–259.

[Spencer 1972] A. J. M. Spencer, *Deformations of fibre-reinforced materials*, Clarendon Press, 1972.

[Spencer 1984] A. J. M. Spencer (editor), *Continuum theory of the mechanics of fibre-reinforced composites*, Courses and lectures / International Centre for Mechanical Sciences **282**, Springer, 1984.

[Spencer and Soldatos 2007] A. J. M. Spencer and K. P. Soldatos, "Finite deformations of fibre-reinforced elastic solids with fibre bending stiffness", *Int. J. Non-Linear Mech.* **42**:2 (2007), 355–368.

[Ting 1996] T. C. T. Ting, *Anisotropic elasticity: theory and applications*, Oxford Engineering Science Series **45**, Oxford University Press, New York, 1996.

[Ye 2003] J. Q. Ye, *Laminated composite plates and shells: 3D modelling*, Springer, 2003.

Received 12 May 2010. Accepted 17 Jul 2010.

MOHAMED A. DAGHER: pmxmd2@nottingham.ac.uk
Theoretical Mechanics, School of Mathematical Sciences, University of Nottingham, University Park, Nottingham, MG7 2RD, United Kingdom

and

Department of Science and Engineering Mathematics, Faculty of Petroleum and Mining Engineering, Suez Canal University, Suez, Egypt

KOSTAS P. SOLDATOS: kostas.soldatos@nottingham.ac.uk
Theoretical Mechanics, School of Mathematical Sciences, University of Nottingham, University Park, Nottingham, MG7 2RD, United Kingdom